
Properties of interstellar filaments as derived from *Herschel*, *Planck*, and molecular line observations

Doris Arzoumanian

DORIS.ARZOUMANIAN@NAGOYA-U.JP

Laboratoire AIM, CEA/DSM–CNRS–Université Paris Diderot, IRFU/Service d’Astrophysique,

C.E.A. Saclay, Orme des Merisiers, 91191 Gif-sur-Yvette, France

Present address: Department of Physics, Graduate School of Science, Nagoya University,

Furo-cho, Chikusa-ku, Nagoya 464-8602, Japan

Abstract

Recent *Herschel* and *Planck* observations of submillimeter dust emission revealed the omnipresence of filamentary structures in the interstellar medium (ISM). The ubiquity of filaments in quiescent clouds as well as in star-forming regions indicates that the formation of filamentary structures is a natural product of the physics at play in the magnetized turbulent cold ISM. An analysis of more than 270 filaments observed with *Herschel* in 8 regions of the Gould Belt, shows that interstellar filaments are characterized by a narrow distribution of central width, while they span a wide column density range. Molecular line observations of a sample of these filaments show evidence of an increase in the velocity dispersion of dense filaments with column density, suggesting an evolution in mass per unit length due to accretion of surrounding material onto these star-forming filaments. The analyses of *Planck* dust polarization observations show that the mean magnetic field along the filaments is different from that of their surrounding clouds. This points to a coupling between the matter and the \vec{B} -field in the filament formation process. These observational results, derived from dust and gas tracers in total and polarized intensity, set strong constraints on theoretical models for filament formation and evolution. They also provide important hints on the initial conditions of the star formation process from the fragmentation of dense (supercritical) filaments. Higher resolution dust polarization observations and large scale molecular line mapping are nevertheless required to investigate in more details the internal structure of interstellar filaments.

1. Omnipresence of filamentary structures in the interstellar medium

While molecular clouds were already known to exhibit filamentary structures (e.g., Schneider & Elmegreen, 1979; Abergel et al., 1994), the omnipresence of filaments in the interstellar medium (ISM) and molecular clouds has only recently been revealed thanks to the high resolution and the high dynamic range of *Herschel* observations of the submillimeter (submm) dust emission (e.g., André et al., 2010; Molinari et al., 2010, and Fig. 1). Furthermore, the all-sky maps of dust submm emission observed by *Planck* in total intensity, as well as in polarized intensity, emphasize the

large-scale, hierarchical filamentary texture of the Galactic ISM (Planck Collaboration Int. XIX, 2015; Planck Collaboration Int. XXXII, 2016). *Herschel* and *Planck* data show that interstellar matter is organized in web-like networks of filaments, which appear to be formed as a natural result of the physics at play in the ISM. The presence of interstellar filaments in both star-forming regions as well as in non-star-forming quiescent clouds, alludes to a formation process of filaments preceding any star-forming activity (André et al., 2010). The spatial distribution of prestellar cores and protostars extracted from *Herschel* images observed mainly along the densest filaments (Könyves et al., 2015) indicates that the properties of interstellar filaments may be a key element defining the initial conditions required for the onset of star formation (André et al., 2014).

Hence, characterizing the observed filament properties in detail, combining tracers of gas and dust in total and polarized intensities is essential to make progress in our understanding of the physical processes involved in the formation and evolution of interstellar filaments and their role in the star formation process.

In the following, I discuss the main results on the properties of interstellar filaments derived from *Herschel*, *Planck*, and molecular line observations. *Herschel* continuum observations are essential to describe the filament (column) density distribution. These data are complemented with ground based molecular line observations to access to the kinematics of the filamentary structures, while *Planck* dust polarization observations give unprecedented information on the structure of the magnetic field and its connection with interstellar matter. These results are presented in the context of a new paradigm of star formation, which is closely linked to the formation and fragmentation of self-gravitating filaments.

2. Filament properties as derived from *Herschel* observations of nearby clouds

Statistical analysis of nearby interstellar filaments has been possible thanks to the *Herschel* Gould Belt survey observations (André et al., 2010), which are ideal to characterize the filament properties, providing the resolution, the sensi-

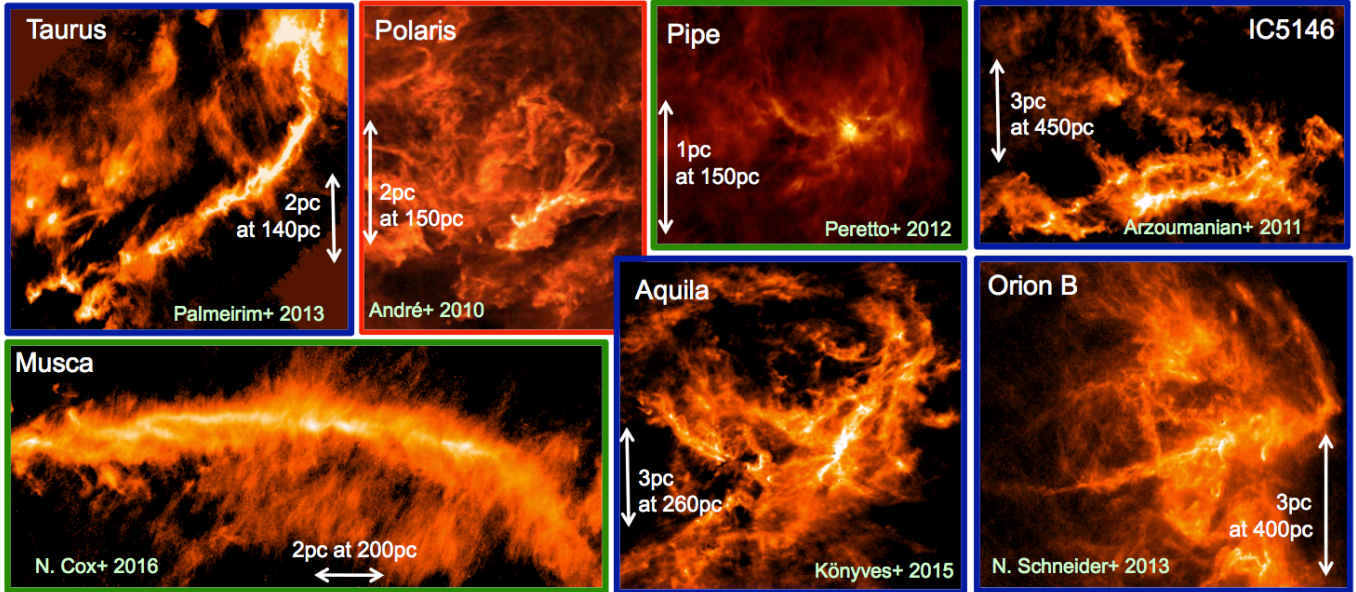


Figure 1. Column density, N_{H_2} [cm^{-2}], maps derived from *Herschel* five-wavelength images [from 70 to 500 μm] observed as part of the *Herschel* Gould Belt survey (André et al., 2010). These seven molecular clouds are framed with colours reflecting their star forming activity: from actively star forming (blue) to mostly quiescent (red).

tivity, and the statistics needed for such studies. *Herschel* observations of a large number of clouds with different star formation activities and environments have been analysed (e.g., Men’shchikov et al., 2010; Peretto et al., 2012; Schneider et al., 2013, and Fig. 1).

Detailed measurements of the radial column density profiles (see Fig. 2-Right) derived from *Herschel* column density maps show that interstellar filaments are characterized by a narrow distribution of central widths, around 0.1 pc (Fig. 2-Left), while they span almost three orders of magnitude in central column density as can be seen on the left hand side of Fig. 3 (Arzoumanian et al., 2011, and Arzoumanian et al., in prep.).

This characteristic filament width (cf., Koch & Rosolowsky, 2015, for an independent analysis) is well resolved by *Herschel* observations of the Gould Belt clouds as can be seen on the radial profile shown in Fig. 2-Right and Fig. 3-Left, where the measurements of the filament widths lie above the horizontal lines corresponding to the resolution limits. This typical filament width of 0.1 pc is also in contrast with the much broader distribution of central Jeans lengths, $\lambda_J \propto c_s^2 / (GN_{\text{H}_2}^0)$, from 0.02 to 1.3 pc (for $T = 10$ K), implying that these filaments are not in hydrostatic equilibrium.

These filaments also span a wide range in mass per unit length (M_{line}), estimated from their column density profiles. The mass per unit length of a filament, is a very important parameter, which defines its “stability”: a fila-

ment is subcritical, unbound when its mass per unit length is smaller than the critical value $M_{\text{line,crit}} = 2c_s^2/G \sim 16 M_{\odot}/\text{pc}$, where $c_s \sim 0.2$ km/s is the isothermal sound speed for $T \sim 10$ K, and G is the gravitational constant (Ostriker, 1964). A filament is supercritical, unstable for radial collapse and fragmentation, when $M_{\text{line}} > M_{\text{line,crit}}$ (Inutsuka & Miyama, 1997).

3. Internal velocity dispersions of interstellar filaments derived from molecular line observations

The total velocity dispersion (σ_{tot}) of selected positions towards a sample of 46 filaments, derived from (^{13}CO , C^{18}O , and N_2H^+) molecular line observations, are presented in Fig. 3–Right. Thermally subcritical and nearly critical filaments have transonic velocity dispersions ($c_s \lesssim \sigma_{\text{tot}} < 2c_s$) independent of column density and are gravitationally unbound. The velocity dispersion of thermally supercritical filaments increases as a function of their column density (roughly as $\sigma_{\text{tot}} \propto N_{\text{H}_2}^{0.5}$). These measurements confirm that there is a critical threshold in M_{line} above which filaments are self-gravitating and below which they are unbound. The position of this threshold, is consistent within a factor of two with the critical value $M_{\text{line,crit}} \sim 16 M_{\odot}/\text{pc}$ for $T=10$ K, equivalent to a column density of $8 \times 10^{21} \text{ cm}^{-2}$ (Arzoumanian et al., 2013).

These observations show that the mass per unit length of supercritical filaments is close to their virial mass per unit

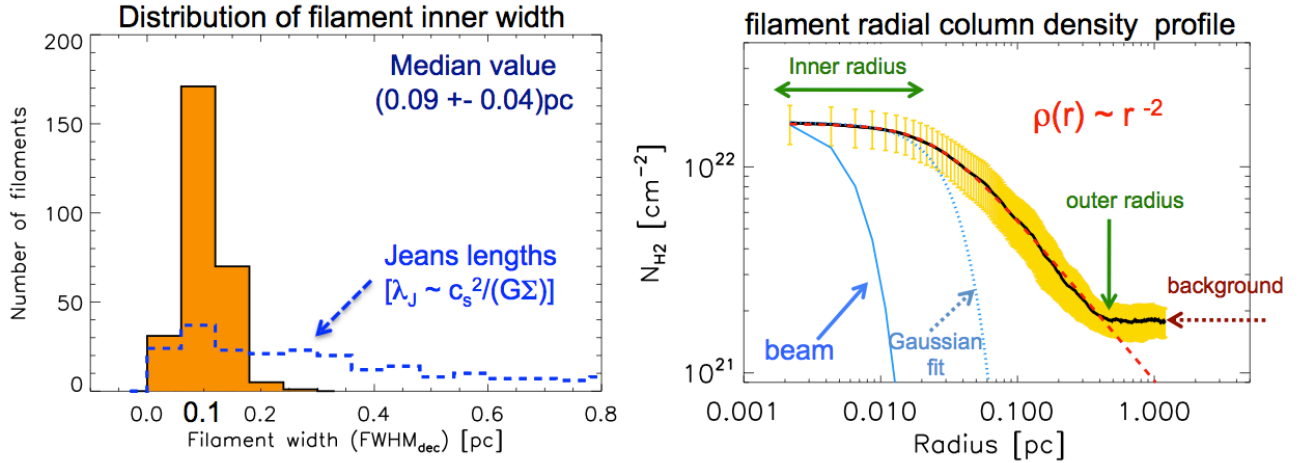


Figure 2. Left: Distribution of deconvolved FWHM widths for 278 filaments observed in 8 different regions (black solid histogram, filled in orange), with a median value of 0.09 ± 0.04 pc. For comparison, the blue dashed histogram represents the distribution of central (thermal) Jeans lengths of the filaments. **Right:** Radial column density profile averaged along the length of the B211/13 filament in Taurus (Palmeirim et al., 2013). The median absolute deviation of the radial profiles along the filament length is shown in yellow. The profile is well fitted with a *Plummer-like* function (red dashed curve) where the density decreases as r^{-2} at large radii (Arzoumanian et al., 2011; Palmeirim et al., 2013).

length $M_{\text{line,vir}} = 2\sigma_{\text{tot}}^2/G$ (Fiege & Pudritz, 2000) where σ_{tot} is the observed total velocity dispersion (instead of the thermal sound speed used in the expression of $M_{\text{line,crit}}$).

We suggest that the large velocity dispersions of supercritical filaments is not a result of the supersonic interstellar turbulence but may be driven by gravitational contraction/accretion (Arzoumanian et al., 2013). Mass accretion is indirectly suggested by transverse velocity gradients observed across a self-gravitating filament in Taurus. The systemic velocities (Goldsmith et al., 2008) of the observed emission in the north and south sides of the filament are redshifted and blueshifted, respectively, with respect to the velocity of the emission observed towards the B211/13 filament (Palmeirim et al., 2013). Such a velocity field pattern may indicate convergence of matter onto the densest parts of the supercritical filament. This is also compatible with theoretical models for the evolution of supercritical filaments (Hennebelle & André, 2013; Heitsch, 2013). Such models put forward the role of continuous accretion, which may be a physical reason to explain the observed properties of supercritical filaments.

4. Magnetic field structure as derived from *Planck* dust polarization observations

Dust polarization observations are essential to infer the orientation of the magnetic field (\vec{B}) component projected on the plane of the sky (POS). While the observed polarization fraction (p) depends on several parameters (dust polarization properties, grain alignment efficiency, and \vec{B} -

field structure, e.g., Hildebrand, 1983), the observed polarization angle (ψ) derived from dust polarized emission is perpendicular to orientation of the \vec{B} -field component on the POS (\vec{B}_{POS}) averaged along the line of sight (LOS). *Planck* observations at 353 GHz provide the first fully sampled maps of the polarized dust emission towards interstellar filaments and their backgrounds, providing unprecedented insight into the \vec{B} -field structure. The first striking result is the impressively ordered structure of \vec{B}_{POS} from the largest Galactic scales down to the smallest scales probed by *Planck* observations, ~ 0.2 pc in nearby molecular clouds (Fig. 4, and Planck Collaboration Int. XIX, 2015; Planck Collaboration Int. XXXV, 2016).

To quantify the polarized intensity observed towards the filaments, we derive radial profiles perpendicular to their crests and averaged along their length to increase the signal-to-noise ratio in polarization, while keeping the highest resolution ($4''.8$) of the *Planck* data. We describe the observations as a two-component model and separate the emission of the filaments from that of their background (surrounding cloud). This allows us to characterize and compare the polarization properties of each emission component: the filament and its background. This is an essential step in measuring the intrinsic polarization fraction (p) and polarization angle (ψ) of each emission component. The analyses show that both the polarization angle and fraction measured at the intensity peak of the filaments (before background subtraction) differ from their intrinsic values (after background subtraction) as described in (Planck Collaboration Int. XXXIII, 2016).

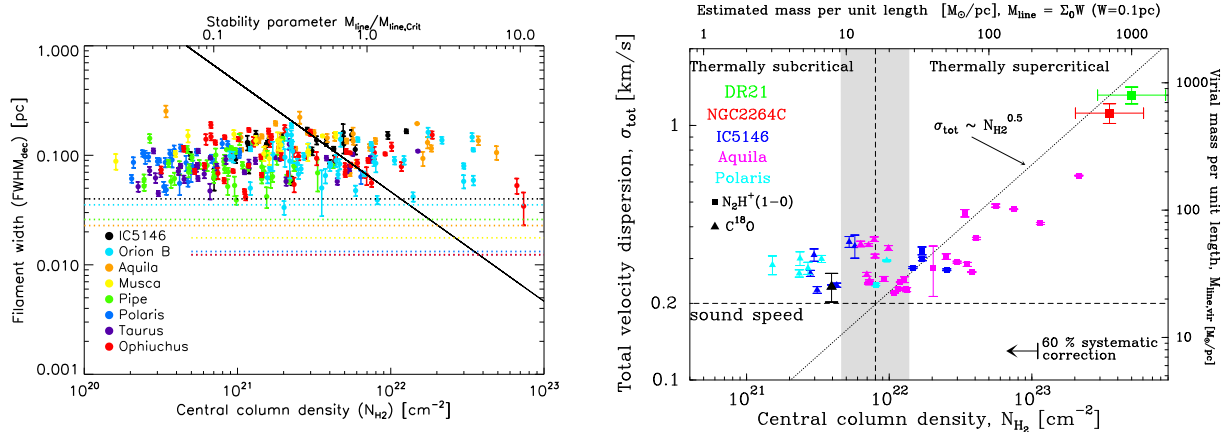


Figure 3. Left: Mean deconvolved width versus background subtracted central column density for the filament sample analysed in 8 regions (indicated on the plot). The spatial resolutions of the column density maps are marked by the horizontal dotted lines. The solid line running from top left to bottom right shows the central Jeans length as a function of central column density. The upper x -axis scale is an estimate of the filament mass per unit length in units of the thermal critical value $M_{\text{line,crit}} = 2c_s^2/G$, where $M_{\text{line}} \propto WN_{\text{H}_2}^0$ with $W = 0.1$ pc (Arzoumanian et al., 2011). **Right:** Filament total velocity dispersion versus observed central column density. The vertical dashed line marks the boundary between thermally subcritical and thermally supercritical filaments where the estimated mass per unit length M_{line} is approximately equal to the critical value $M_{\text{line,crit}} \sim 16 M_{\odot}/\text{pc}$ for $T=10$ K, equivalent to a column density of $8 \times 10^{21} \text{ cm}^{-2}$. The grey band shows a dispersion of a factor of 3 around this nominal value. The dotted line running from the bottom left to the top right corresponds to $\sigma_{\text{tot}} \propto N_{\text{H}_2}^{0.5}$ (Arzoumanian et al., 2013).

The left panel of Fig. 5 shows the profile of ψ across the Musca, B211, and L1506 filaments. In all three cases, we measure variations in the polarization angle intrinsic to the filaments (ψ_{fil}) with respect to that of their backgrounds (ψ_{bg}). These variations are found to be coherent along the pc-scale length of the filaments. The differences between ψ_{fil} and ψ_{bg} for two of the three filaments are larger than the dispersion of the polarization angles across and along the filaments (see Table 2 in Planck Collaboration Int. XXXIII, 2016). Hence, these differences are not random fluctuations and they indicate a change in the orientation of the POS component of the magnetic field between the filaments and their backgrounds.

The observations show a decrease in the polarization fraction p from the background to the Musca filament (Fig. 5–right), as well as towards the Taurus B211 and L1506 filaments (see Fig. 10 of Planck Collaboration Int. XXXIII, 2016). A decrease in p with the total column density N_{H} (i.e., from the backgrounds to the filament crests), has been already shown in previous studies. This decrease has been usually interpreted as due to the turbulent component of the field and/or variations of dust alignment efficiency with increasing column density (e.g., Whittet et al., 2008; Jones et al., 2015, and references therein). In our study, the bulk of the drop in p within the filaments cannot be explained by random fluctuations of the orientation of the magnetic field because they are too small ($\sigma_{\psi} < 10^\circ$). We argue that the observed drop in p towards the filaments may be due to the 3D structure of the magnetic field: both its orientation

in the POS and with respect to the POS (Planck Collaboration Int. XXXIII, 2016). Indeed, the observed changes of ψ are direct evidence of variations of the orientation of the POS projection of the magnetic field. The systematic variations of ψ suggest changes of the angle of the magnetic field with respect to the POS. This angle must statistically vary as much as ψ , contributing to the observed decrease of p in the filaments. The observed variation of ψ between the filaments and their backgrounds always depolarizes the total emission, due to the integration of the emission along the LOS of two emission components where the angle of \vec{B}_{POS} varies (see Fig. 5 and Planck Collaboration Int. XXXIII, 2016).

The inner structure of the filaments (as seen, e.g., with *Herschel*, cf., Palmeirim et al., 2013; Cox et al., 2016), is not resolved, but at the smallest scales accessible with *Planck* (~ 0.2 pc towards the nearby clouds), the observed changes of ψ and p (derived from *Planck* polarization data at the resolution of $4'8$) hold some information on the magnetic field structure within filaments (Planck Collaboration Int. XXXIII, 2016). They show that both the mean field and its fluctuations in the filaments are different from those in the background clouds, which points to a coupling between the matter and the \vec{B} -field in the filament formation process.

5. Summary and conclusions

The ubiquity of filaments in both quiescent clouds and active star-forming regions, where they are associated with

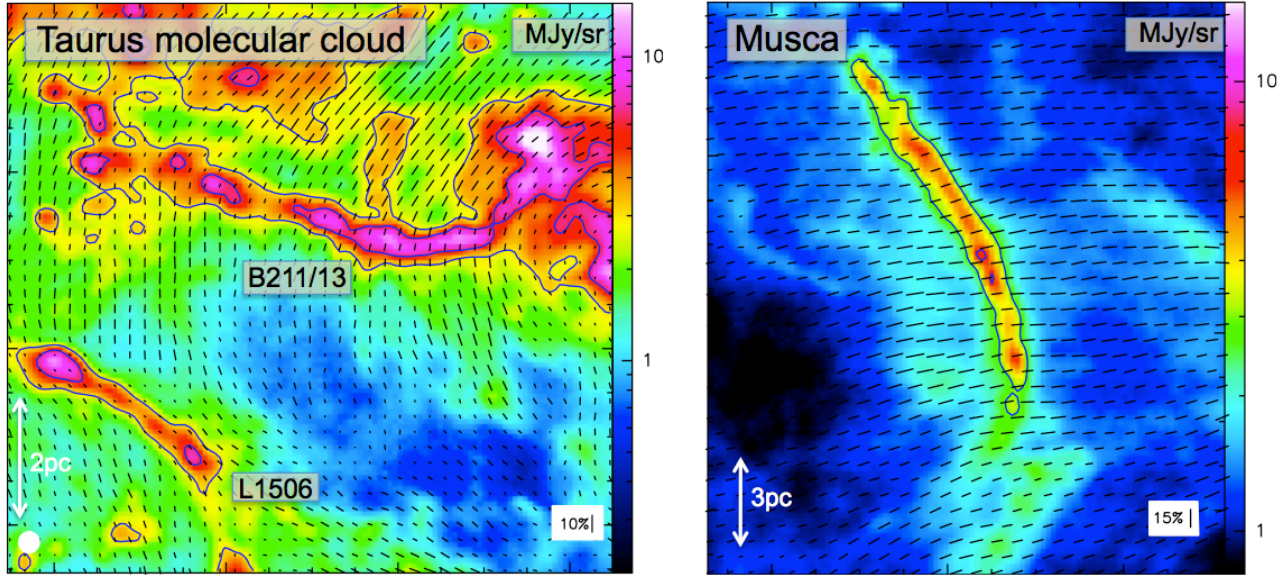


Figure 4. *Planck* 353 GHz ($850\ \mu\text{m}$) total dust intensity (Stokes I) maps at a resolution of $4''.8$, towards the Taurus B211/13 and L1506 filaments (**Left**) and the Musca filament (**Right**). The maps are in Galactic coordinate system. The blue contours show the levels of 3 and $6\ \text{MJy sr}^{-1}$. The black segments show the \vec{B}_{POS} -field orientation ($\psi+90^\circ$). The length of the pseudo-vectors is proportional to the polarization fraction. The polarization angles and fractions are computed at a resolution of $9''.6$ (indicated by the white filled circles on the left hand side map) for increased S/N (*Planck* Collaboration Int. XXXIII, 2016).

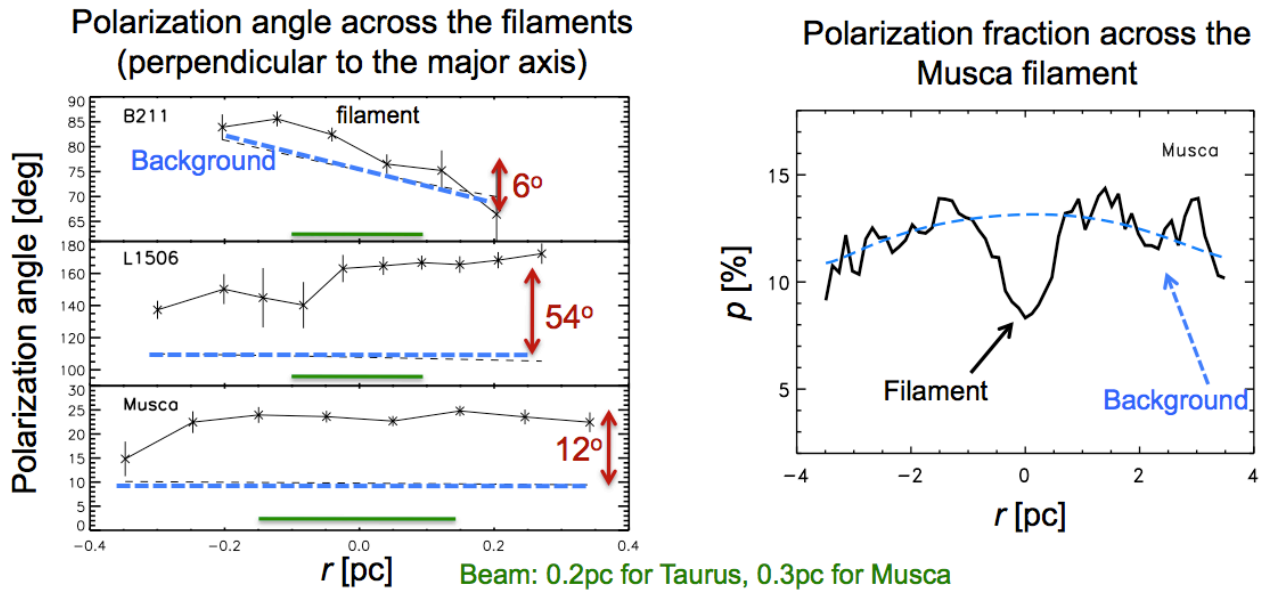


Figure 5. **Left:** Filament intrinsic polarization angle (tracing the angle of \vec{B}_{POS}) across the crests of the B211, L1506, and Musca filaments. The x -axis shows the radial distance from the filament crest. The crosses are data points computed from Q and U background subtracted maps. The dashed line represents the background polarization angle. The difference between the polarization angle of the filament and that of the background is indicated on the plots (taken from Table 2 in *Planck* Collaboration Int. XXXIII, 2016). **Right:** Observed profile (in black) of the polarization fraction (p) perpendicular to the crest of the Musca filament. The dashed blue curve shows the polarization fraction of the background. It is derived from the Stokes I , Q , and U parameters of the background.

the presence of prestellar cores and protostars (Könyves et al., 2015), supports the view that filaments are (first) form in the ISM and the densest of them fragment into star-forming cores (André et al., 2014). The observational finding of a filament uniform 0.1 pc width (Arzoumanian et al., 2011) sets strong constraints on the physics at play in the ISM. This result has been recently observed (at higher-resolution) from the ground in regions farther away than the Gould Belt (Hill et al., 2012; André et al., 2016).

Interestingly 0.1 pc corresponds to the sonic scale below which interstellar turbulence becomes subsonic in diffuse, non-star-forming gas. This occurrence, along with the observed thermal velocity dispersion of low column density filaments, suggests that large-scale turbulence may be a main player in the formation of the filamentary web observed in molecular clouds (Arzoumanian et al., 2011). On the other hand, the increase of the non-thermal velocity dispersion of supercritical, self-gravitating filaments, with column density, may indicate the generation of internal turbulence due to gravitational accretion. This may be an explanation for the observed constant width of self-gravitating collapsing filaments (Arzoumanian et al., 2013).

While the dissipation of interstellar turbulence provides a plausible mechanism for filament formation, the observed organization between the magnetic field lines and the intensity structures, derived from the analysis of *Planck* data, indicates that the \vec{B} -field plays a dynamically important role in shaping the interstellar matter (Planck Collaboration Int. XXXIII, 2016; Planck Collaboration Int. XXXV, 2016). In particular, they may be a key element to understand the channel of mass flows in the ISM. The fact that most prestellar cores lie in dense, self-gravitating filaments (Könyves et al., 2015) suggests that gravity is a major driver in the evolution of supercritical filaments and their fragmentation in star-forming prestellar cores.

The combination of these observational results, derived from dust and gas tracers in total and polarized intensity, give strong constraints on our understanding of the formation and evolution of filaments in the ISM, which provides important clues to the initial conditions of the star formation process along supercritical filaments. Higher resolution dust polarization observations and large scale molecular line mapping are nevertheless required to investigate in more details the internal velocity and magnetic field structures of interstellar filaments.

Acknowledgments

DA has received support from the European Research Council grant ORISTARS (No. 291294) and is currently an International Research Fellow of the Japan Society for the Promotion of Science (FY2016).

References

- Abergel, A., Boulanger, F., Mizuno, A., & Fukui, Y. 1994, *ApJ*, 423, L59
- André, P., Di Francesco, J., Ward-Thompson, D., et al. 2014, in *Protostars and Planets VI*, p. 27
- André, P., Men'shchikov, A., Bontemps, S., et al. 2010, *A&A*, 518, L102
- André, P., Révêret, V., Könyves, V., et al. 2016, *A&A*, 592, A54
- Arzoumanian, D., André, P., Peretto, N., & Könyves, V. 2013, *A&A*, 553, A119
- Arzoumanian, D., André, P., Didelon, P., et al. 2011, *A&A*, 529, L6
- Cox, N. L. J., Arzoumanian, D., André, P., et al. 2016, *A&A*, 590, A110
- Fiege, J. D., & Pudritz, R. E. 2000, *MNRAS*, 311, 85
- Goldsmith, P. F., Heyer, M., Narayanan, G., et al. 2008, *ApJ*, 680, 428
- Heitsch, F. 2013, *ApJ*, 769, 115
- Hennebelle, P., & André, P. 2013, *A&A*, 560, A68
- Hildebrand, R. H. 1983, *QJRAS*, 24, 267
- Hill, T., Andre, P., Arzoumanian, D., et al. 2012, *A&A*, 548, L6
- Inutsuka, S., & Miyama, S. M. 1997, *ApJ*, 480, 681
- Jones, T. J., Bagley, M., Krejny, M., Andersson, B.-G., & Bastien, P. 2015, *AJ*, 149, 31
- Koch, E. W., & Rosolowsky, E. W. 2015, *MNRAS*, 452, 3435
- Könyves, V., André, P., Men'shchikov, A., et al. 2015, *A&A*, 584, A91
- Men'shchikov, A., André, P., Didelon, P., et al. 2010, *A&A*, 518, L103+
- Molinari, S., Swinyard, B., Bally, J., et al. 2010, *A&A*, 518, L100
- Ostriker, J. 1964, *ApJ*, 140, 1056
- Palmeirim, P., André, P., Kirk, J., et al. 2013, *A&A*, 550, A38
- Peretto, N., André, P., Könyves, V., et al. 2012, *A&A*, 541, A63
- Planck Collaboration Int. XIX. 2015, *A&A*, 576, A104
- Planck Collaboration Int. XXXII. 2016, *A&A*, 586, A135
- Planck Collaboration Int. XXXIII. 2016, *A&A*, 586, A136
- Planck Collaboration Int. XXXV. 2016, *A&A*, 586, A138
- Schneider, N., André, P., Könyves, V., et al. 2013, *ApJ*, 766, L17
- Schneider, S., & Elmegreen, B. G. 1979, *ApJS*, 41, 87
- Whittet, D. C. B., Hough, J. H., Lazarian, A., & Hoang, T. 2008, *ApJ*, 674, 304